

Experimentally Motivated Order of Length Scales Affect Shot Noise

Sourav Manna^{1,2,*} and Ankur Das^{3,1,†}

¹*Department of Condensed Matter Physics, Weizmann Institute of Science, Rehovot 7610001, Israel*

²*Raymond and Beverly Sackler School of Physics and Astronomy, Tel-Aviv University, Tel Aviv 6997801, Israel*

³*Department of Physics, Indian Institute of Science Education and Research (IISER) Tirupati, Tirupati 517619, India*

Shot noise at a conductance plateau in a quantum point contact (QPC) can be explained by considering equilibrations at the quantum Hall edges. The indication from recent experiments is that the charge equilibration length is much shorter than the thermal equilibration length. We discuss how this discovery gives rise to different thermal equilibration regimes in the presence of full charge equilibration. In this work, we classify these distinct regimes via dc current-current correlations (*electrical shot noise*) at definite experimentally found (or possible) QPC conductance plateaus for the edges of integer, particle-like, and hole-like filling fractions in a two dimensional electron gas. Our analyses show that distinct universal features arise among the different thermal equilibration regimes for the edges of particle-like and hole-like states.

I. INTRODUCTION

Quantum Hall effect is one of the oldest known phenomena that requires understanding of band topology and quantum mechanics [1–5]. However, the bulk-boundary correspondence [6] does not guarantee a comprehensive understanding of the edges for a given bulk topological order. While the bulk is gapped, the edges are gapless which participate in both electrical and thermal transport carrying both charge and energy respectively. The edge modes can be either co-propagating or counter-propagating and can exhibit a distinct steady state. Thus, we can separate our question of the quantum Hall effect into two different pieces: (1) the topological order of the bulk and (2) the details (for example the steady state) of the edge. There is more than one known mechanism that can make the picture of the edge “fuzzy” keeping the bulk-boundary correspondence intact.

One of the phenomena that plagued the quantum Hall edge theory is the edge reconstruction. This is an “umbrella-term” that includes the appearance of new counter-propagating modes [7–9], reordering of the edge modes [10], emergence of an effective narrow strip of spin rotation [11], and more. This was first discussed for the two dimensional electron gas (2DEG) by Chamon and Wen [12] almost three decades ago. They explained how the sharpness of the confining potential can cause the appearance of new counter-propagating edge modes. Following this, there have been numerous efforts to understand the edge reconstruction for integer and fractional quantum Hall systems [13]. More recently, we have learned that even integer quantum Hall edges can have a fractional edge reconstruction [8]. The general answer to the question of when and how edge reconstruction takes place is a non-universal one. This makes the study of edge reconstruction a difficult and detailed topic of interest for both the experimentalists and theorists.

Typically in an experiment, a dc voltage is used as the source which causes voltage drops near different contacts. This gives rise to the Joule heating which produces heat and the heating effects can play a crucial role in the edge transport. Heat, which propagates along the edge modes, induces particle-hole pairs and thermally activates the tunneling of particles and holes among the edge modes. This gives rise to a remarkable phenomenon known as the edge equilibration [14–21]. Such an incoherent phenomenon leads the steady state of edges to a hydrodynamic regime and the edge modes are equilibrated to a hydrodynamic mode of a given chirality. Such a mode is characterized by its electrical and thermal conductances. Tunneling of particles and holes allows the exchange of both charge and heat. This leads to the electro-chemical potential and thermal equilibrations, respectively [14, 19, 20]. The particle-hole pairs can split stochastically into two modes and move into opposite directions in the case of the edges comprising of counter-propagating modes. This mechanism gives rise to the electrical shot noise (current-current correlations), which provides a fully electrical approach to capture the effect of heat propagation along the edges.

In electrical current, there can be fluctuations due to the stochastic injection of particles or holes. Now, the topological properties of a quantum Hall edge allows only certain types of quasi-particle tunnelings to take place, which in turn allows the measurement of quasi-particle charge. Quantum point contact (QPC), described below (c.f. Fig. 1), is one of the ways to generate this stochastic tunneling [22–29]. However, this is not the only mechanism that can generate shot noise. For example, the decay of neutralons (quanta of the neutral modes) can be one of those mechanisms [8, 30–32]. We will discuss another mechanism due to the equilibration later.

Now, the natural question will be how to poke the properties of the edge modes beyond the topological charge and thermal conductances. One of the established techniques is to push the opposite edges of a quantum Hall system close to each other so that they start to tunnel. This is done by an electrostatic constriction, namely a QPC. In the context of the quantum Hall ef-

* sourav.manna@weizmann.ac.il

† ankur@labs.iisertirupati.ac.in

fect, a QPC plays a pivotal role in understanding the microscopic structure of the edge. There are at least two types of measurements one can do in a QPC device : (1) transport and (2) shot noise. As the QPC constriction gets narrower, less current will transmit across the QPC. Now one question can be asked if we find that the transmission remains constant (leading to a transmission plateau) as we make the constriction narrower [33, 34]. In that case, there can be at least two possible scenarios: (1) there are more than one coherently propagating edge modes, and a few of them completely backscatter, while the others fully transmit across the QPC and (2) at the QPC constriction, a very small region of a quantum Hall liquid of a different filling fraction is stabilized such that when these modes electrically equilibrate (incoherent regime), it leads to a transmission plateau. We can also ask if there are any shot noise signatures of these scenarios other than the transport measurements.

In recent times, there have been immense development in QPC and sample standardizations and we have learned that we must treat the equilibration scenario more carefully. What we have learned is that there are *two different* internal length scales involved here, namely the electro-chemical potential or charge equilibration length ($l_{\text{eq}}^{\text{ch}}$) and the thermal equilibration length ($l_{\text{eq}}^{\text{th}}$). Latest experiments have demonstrated that they are not of the same order of magnitude [35–38]. There are two geometric length scales in a QPC geometry (c.f. Fig. 1): (1) length of the arms (L_A) and (2) size of the QPC (L_Q). We know that $L_A \gg L_Q$ and from the experiments [35–38] we have $l_{\text{eq}}^{\text{ch}} \ll l_{\text{eq}}^{\text{th}}$. To have a transmission plateau we must have $l_{\text{eq}}^{\text{ch}} \ll (L_A, L_Q)$ leading to the full charge equilibration in every segment of the QPC geometry. However, the degree of thermal equilibration can be in a distinct regime in different segments. Thus, the interplay among the order of magnitudes of $l_{\text{eq}}^{\text{th}}$, L_A , L_Q leads to distinct inequalities giving rise to a zoo of scenarios. We study the effect of these inequalities in the electrical shot noise (defined below). We point out that the present work goes significantly beyond our earlier works [18, 39, 40] as follows. Ref. 18 deals with a device based on interfacing different quantum Hall filling—thereby the electrical conductance plateaus are defined by the gated regions, whereas in our present work we study a QPC geometry where an electrical conductance plateau originates from the edge structure of the corresponding bulk filling. We considered only full and partial thermal equilibrations in Ref. 18, eliminating any effect of edge reconstruction, whereas in our present work we considered no, hybrid ($L_Q \ll l_{\text{eq}}^{\text{th}} \ll L_A$), and full thermal equilibrations and thereby the effect of edge reconstruction is present. Notably, the hybrid thermal equilibration scenario is not possible in Ref. 18 since we considered an interface-based device there. We considered the 5/2 bulk filling in Ref. 18, which is a particle-hole symmetric state and here, we have studied the states having no particle-hole symmetry. In Refs. 39 and 40, we considered only 2/3 quantum Hall bulk filling, whereas in our present work we go beyond

that and study other Abelian bulk filling factors.

We refer to Fig. 1 for a schematic picture of the QPC geometry and the corresponding transport and shot noise measurements. We have I_1 and I_2 as the currents which enter the drains D_1 and D_2 , respectively. We define the dc current-current auto-correlations as $\delta^2 I_1$ in D_1 , $\delta^2 I_2$ in D_2 , and the cross-correlation as $\delta^2 I_c$ [41] where

$$\begin{aligned}\delta^2 I_1 &= \langle (I_1 - \langle I_1 \rangle)^2 \rangle, \\ \delta^2 I_2 &= \langle (I_2 - \langle I_2 \rangle)^2 \rangle, \\ \delta^2 I_c &= \langle (I_1 - \langle I_1 \rangle)(I_2 - \langle I_2 \rangle) \rangle.\end{aligned}\quad (1)$$

The shot noise Fano factors are defined as

$$F_j = \frac{\delta^2 I_j}{2eI_S t(1-t)}, \quad j \in \{1, 2, c\} \quad (2)$$

where I_S is the source current and $t = I_1/I_S$ is the QPC transmission.

In the following sections, we describe the keynote points of our work (Section II), the assumptions and techniques we use (Section III), and our insight into the results (Section IV). We draw a summary and the future prospect of our work in Section VII.

II. KEYNOTE POINTS

Being motivated by the experiments [34, 42] and previously studied cases [18, 39, 40], we analyze the effects of different orders of length scales on the shot noise signatures and compare the corresponding different Fano factors in full completeness. Here, we not only do a qualitative analysis but also calculate the quantitative values of the Fano factors for all the cases considering the inequalities among $l_{\text{eq}}^{\text{ch}}$, $l_{\text{eq}}^{\text{th}}$, L_A , L_Q . As we do not have any control over the internal length scales, we consider different reasonable scenarios. Below we discuss the keynote points of our results relating one another and explicitly stressing their importance.

Depending on whether the quantum Hall bulk filling is particle-like or hole-like, the edge contains either co-propagating or counter-propagating modes respectively, arising from the topology. Naturally, question arises whether such difference in the edge structure leaves its impressions in shot noise in different equilibration regimes. Indeed, in these results (c.f. Table I), we find interesting structures in the Fano factors for different regimes. We find that the $\nu =$ particle-like and $\nu =$ hole-like states (c.f. Table II) behave *differently* in their shot noise signatures.

Immediate consequences of different regimes of thermal equilibrations are manifested in the shot noise for distinct bulk fillings—particle-like or hole-like. Namely, the Fano factor values for the $\nu =$ particle-like states are the same for the “No” and “Hybrid” thermal equilibrations (arms are thermally equilibrated while edges around the QPC are not thermally equilibrated) for a

ν	ν_i	No equilibration ($F_1 = F_2, F_c$)	Hybrid equilibration ($F_1 = F_2, F_c$)	Full equilibration ($F_1 = F_2, F_c$)
1	1/3	$\approx (0.36, -0.36)$	$\approx (0.36, -0.36)$	$\approx (0.55\sqrt{l_{\text{eq}}^{\text{th}}/L_Q}, -0.55\sqrt{l_{\text{eq}}^{\text{th}}/L_Q})$
	2/3	$\approx (0.33, -0.33)$	$\approx (0.33, -0.33)$	$\approx (0.55\sqrt{l_{\text{eq}}^{\text{th}}/L_Q}, -0.55\sqrt{l_{\text{eq}}^{\text{th}}/L_Q})$
2/5	1/3	$\approx (0.1, -0.1)$	$\approx (0.1, -0.1)$	$\approx (0.0, -0.0)$
3/7	1/3	$\approx (0.086, -0.086)$	$\approx (0.086, -0.086)$	$\approx (0.0, -0.0)$
	2/5	$\approx (0.066, -0.066)$	$\approx (0.066, -0.066)$	$\approx (0.0, -0.0)$
2/3	1/3	$\approx (0.35, -0.22)$	$\approx (0.09 + 0.3\sqrt{L_A/l_{\text{eq}}^{\text{th}}}, 0.09 - 0.3\sqrt{L_A/l_{\text{eq}}^{\text{th}}})$	$\approx (0.09 + 0.3\sqrt{L_A/l_{\text{eq}}^{\text{th}}}, 0.09 - 0.3\sqrt{L_A/l_{\text{eq}}^{\text{th}}})$
	[1/3]	$\approx (0.28, -0.1)$	$\approx (0.09 + 0.3\sqrt{L_A/l_{\text{eq}}^{\text{th}}}, 0.09 - 0.3\sqrt{L_A/l_{\text{eq}}^{\text{th}}})$	$\approx (0.09 + 0.3\sqrt{L_A/l_{\text{eq}}^{\text{th}}}, 0.09 - 0.3\sqrt{L_A/l_{\text{eq}}^{\text{th}}})$
3/5	1/3	$\approx (0.37, -0.097)$	$\approx (0.53, -0.31)$	$\approx (0.53, -0.31)$
	2/5	$\approx (0.38, -0.09)$	$\approx (0.52, -0.3)$	$\approx (0.52, -0.3)$
4/7	1/3	$\approx (0.39, -0.01)$	$\approx (0.39, -0.19)$	$\approx (0.39, -0.19)$
	2/5	$\approx (0.43, -0.009)$	$\approx (0.39, -0.18)$	$\approx (0.39, -0.18)$
	3/7	$\approx (0.45, -0.008)$	$\approx (0.39, -0.17)$	$\approx (0.39, -0.17)$

TABLE I. Summary of our shot noise results : F_1, F_2 are the auto-correlation Fano factors for the drains D_1, D_2 , respectively, while F_c is the cross-correlation Fano factor for different bulk filling factor ν and QPC filling factor $\nu_i (< \nu)$ in distinct thermal equilibration regimes namely “No”, “Hybrid”, and “Full”. We assume full charge equilibration and different degree of thermal equilibration in each of the segments L_A, L_Q (c.f. Fig. 2). We always have $F_1 = F_2$, but F_c is not always equal in magnitude to $F_1 = F_2$. For the $\nu =$ particle-like states, “No” and “Hybrid” thermal equilibrations have the same values for $F_1 = F_2, F_c$ (shaded pink) for a given $\{\nu, \nu_i\}$. Similarly, for the $\nu =$ hole-like states we find that $F_1 = F_2, F_c$ acquire the same values for “Hybrid” and “Full” thermal equilibrations (shaded blue) for a given $\{\nu, \nu_i\}$. Here, $l_{\text{eq}}^{\text{th}}$ denotes the thermal equilibration length and ≈ 0 indicating an exponential suppression as a function of the geometric lengths. We mention that $\{\nu, \nu_i\} = \{2/3, [1/3]\}$ denotes the 1/3 edge reconstruction in $\nu = 2/3$ [7] and the results for $\nu = 2/3$ also appear in [39, 40]. For a given bulk filling fraction, either 3/5 or 4/7, we note the following. Corresponding to a given QPC filling, while $F_1 = F_2$ are numerically close for different thermal equilibration regimes, however, F_c differs significantly by order of magnitude. Hence, this can facilitate the experimental detection. Notably, F_c is routinely measured in different experiments [43, 44].

given $\{\nu, \nu_i\}$, where $\nu_i (< \nu)$ is the QPC filling. This is because all the modes are co-propagating, and equilibrating those in the arm (“outer” segment) does not make a difference (c.f. Fig. 3(a)). However, the situation changes for the $\nu =$ hole-like states where the Fano factors for the “Hybrid” and “Full” thermal equilibrations are equal for a given $\{\nu, \nu_i\}$. This is because the counter-propagating modes in the arm (“outer” segment) make sure that all the heat from a hot spot reaches the noise spots for both the “Hybrid” and “Full” thermal equilibration regimes (c.f. Fig. 3(b)).

Now, the degree of thermal equilibration also leaves a profound impact on the heat transport of a given segment, which in turn shows up on the geometric length dependence of the shot noise. The Fano factors can be exponentially suppressed (as a function of the geometric lengths) or constant or length dependent depending on the nature of heat transport (ballistic or antiballistic or diffusive, respectively) in different segments of the QPC geometry. Moreover, due to the antiballistic heat transport we also find that for all the $\nu =$ hole-like states, the auto- and the cross-correlation Fano factors are *not equal*. Though it is not expected from the conventional picture of the shot noise at a QPC geometry but can be understood in the equilibration picture.

Thus, this work provides a comprehensive study, as summarized in Table I, of the shot noise Fano factors where (1) we take the order of internal lengths $l_{\text{eq}}^{\text{ch}}, l_{\text{eq}}^{\text{th}}$ seriously including their comparison with the geometric lengths L_A, L_Q and (2) we find qualitative inequalities for the different Fano factors (besides quantitative values)

resolving distinct scenarios.

III. ASSUMPTIONS AND TECHNIQUES

Taking into considerations the recent experiments [35–38], showing that the thermal equilibration length is order of magnitude larger than the charge equilibration length, and the typical geometric lengths of a QPC geometry (where arm length is much larger than the QPC size) we believe and consider the following three distinct relevant possibilities (c.f. Fig. 2) :

1. $l_{\text{eq}}^{\text{th}} \ll L_Q \ll L_A$: “Full” thermal equilibration regime, where the system is fully thermally equilibrated in every segment.
2. $L_Q \ll l_{\text{eq}}^{\text{th}} \ll L_A$: “Hybrid” thermal equilibration regime, where the system is fully thermally equilibrated in the arms but thermally unequibrated around the QPC.
3. $L_Q \ll L_A \ll l_{\text{eq}}^{\text{th}}$: “No” thermal equilibration regime, where the system is not thermally equilibrated in any segment.

We will focus our analysis on these aforementioned cases and assume $l_{\text{eq}}^{\text{ch}} \ll (L_A, L_Q)$ providing full charge equilibration in each segment of the QPC geometry.

We use Refs. 18, 20, 39, and 40 and write the general expressions for the auto- and cross-correlations in a QPC geometry for the bulk filling ν and QPC filling ν_i

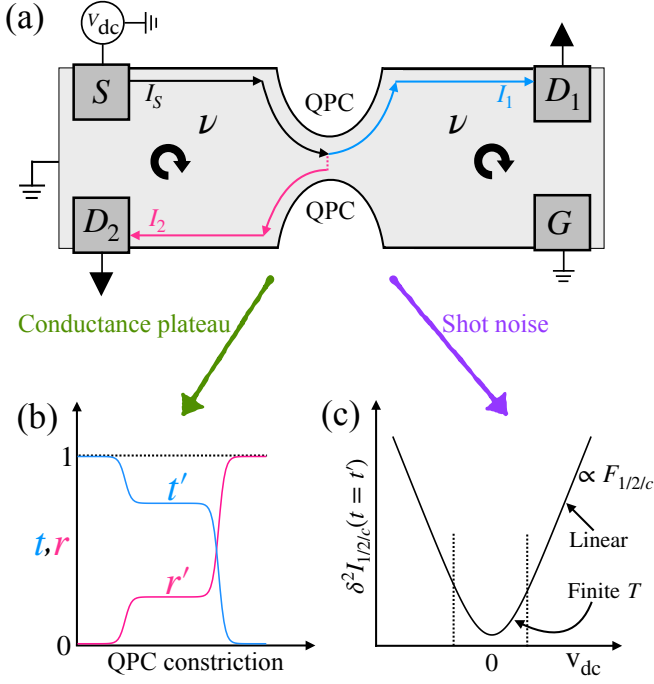


FIG. 1. A schematic picture of the device and measurements, which we use throughout the paper. (a) We show a Hall bar with filling ν in a QPC geometry. We have four contacts as a source S , a ground G , and two drains D_1, D_2 . A dc current I_S is injected by S , which is biased by a dc voltage V_{dc} , and the measurements are performed at D_1, D_2 . We describe the chirality of charge propagation by circular arrows. (b) Transport measurements are carried out by measuring currents I_1, I_2 at D_1, D_2 respectively. The transmission and reflection coefficients are $t = I_1/I_S$ and $r = I_2/I_S$ respectively, where $t+r = 1$. A QPC transmission plateau can be observed at a transmission $t = t'$ while measuring t (correspondingly r) as a function of the QPC constriction (from a fully open to a fully pinched off QPC). (c) At a transmission plateau ($t = t'$), the current reaching D_1, D_2 can be noisy (leading to $\delta^2 I_{1/2/c}(t = t') \neq 0$) and there can be different mechanisms to it. The functional dependence of $\delta^2 I_{1/2/c}(t = t')$ is schematically shown while changing V_{dc} and the slope of the linear region is proportional to the corresponding Fano factor $F_{1/2/c}$. The curvature in $\delta^2 I_{1/2/c}(t = t')$ shows up due to the temperature dependence.

when $\nu > \nu_i$ (Fig. 2 and Fig. 3). Charge is assumed to be fully equilibrated, leading to a ballistic charge transport, moving “downstream” along each segment of the QPC geometry. We define antiballistic as the direction opposite to the charge flow (“upstream”). We use those expressions to compute the correlation values for various choices of $\{\nu, \nu_i\}$ and for different thermal equilibration regimes under considerations assuming no bulk-leakage [15, 17, 45, 46]. We write the $\delta^2 I_1, \delta^2 I_2$, and $\delta^2 I_c$ as

$$\delta^2 I_1 = 2 \left(\frac{e^2}{h} \right) \frac{\nu_i}{\nu} (\nu - \nu_i) k_B (T_M + T_N) + \frac{1}{\nu^2} \left[\nu_i^2 \langle (\Delta I_S)^2 \rangle + (\nu - \nu_i)^2 \langle (\Delta I_G)^2 \rangle \right], \quad (3)$$

$$\delta^2 I_2 = 2 \left(\frac{e^2}{h} \right) \frac{\nu_i}{\nu} (\nu - \nu_i) k_B (T_M + T_N) + \frac{1}{\nu^2} \left[\nu_i^2 \langle (\Delta I_G)^2 \rangle + (\nu - \nu_i)^2 \langle (\Delta I_S)^2 \rangle \right], \quad (4)$$

$$\delta^2 I_c = -2 \left(\frac{e^2}{h} \right) \frac{\nu_i}{\nu} (\nu - \nu_i) k_B (T_M + T_N) + \frac{\nu_i (\nu - \nu_i)}{\nu^2} \left[\langle (\Delta I_G)^2 \rangle + \langle (\Delta I_S)^2 \rangle \right], \quad (5)$$

where T_M, T_N are the temperatures at the noise spots M and N , respectively. The corresponding Fano factors can be found by using Eq. (2). We find T_M, T_N by solving self-consistent equilibration equations and considering energy conservations [18, 20, 39, 40]. Owing to the Joule heating, power is dissipated at the hot spots as

$$P_{H_1} = P_{H_2} = \frac{e^2 V_{dc}^2}{h} \frac{\nu_i (\nu - \nu_i)}{2\nu}. \quad (6)$$

We compute the contributions $\langle (\Delta I_G)^2 \rangle = \langle (\Delta I_S)^2 \rangle$ at the noise spots O and P by evaluating the following integral ([18, 20]) as

$$\begin{aligned} \langle (\Delta I_S)^2 \rangle &= \langle (\Delta I_G)^2 \rangle \\ &= \frac{2e^2}{h l_{eq}^{ch}} \nu \frac{\nu_-}{\nu_+} \int_0^{L_A} dx \frac{e^{-\frac{2x}{l_{eq}^{ch}}} k_B [T_+(x) + T_-(x)]}{[1 - (e^{-\frac{-L_A}{l_{eq}^{ch}}} \frac{\nu_-}{\nu_+})]^2}, \end{aligned} \quad (7)$$

where l_{eq}^{ch} is the charge equilibration length and $\nu = (\nu_+ - \nu_-)$. We have ν_+ and ν_- as the filling factors of the downstream and upstream modes, respectively. Here $T_{\pm}(x)$ are the temperature profiles of the modes with filling factors ν_{\pm} , respectively. We note that $T_{\pm}(x)$ depend on the l_{eq}^{th} and we find these by following Ref. 20. We assume that no voltage drops occur along the “outer” segment (Fig. 3) and

$$T_+(0) = 0, \quad T_-(L_A) = T_M \quad (8)$$

serve as the boundary conditions since we consider that the lead contacts are at zero temperature. We point out that, the “No” thermal equilibration regime was also studied in Ref. 37 for one edge segment. We note that in this regime, only the upstream modes from $M(N)$ contribute to $O(P)$, but the downstream modes do not contribute (Fig. 3(b)). This is because the downstream

ν	Edge structure	ν	Edge structure
1	$\nu = 0$ $\nu = 1$	2/3	(a) $\nu = 0$ $\nu = 2/3$ (b) $\nu = 0$ $\nu = 2/3$ $1/3$ $1/3$ $1/3$
2/5	$\nu = 0$ $\nu = 2/5$	3/5	$\nu = 0$ $\nu = 3/5$ $1/15$ $1/15$
3/7	$\nu = 0$ $\nu = 3/7$	4/7	$\nu = 0$ $\nu = 4/7$ $1/35$ $1/35$ $1/35$

TABLE II. We show the edge structures of integer ($\nu = 1$), particle-like ($\nu = 1/3, 2/5, 3/7$), and hole-like ($\nu = 2/3, 3/5, 4/7$) filling fractions under considerations. Integer and fractional charge modes are depicted as double and single-headed arrows respectively. Each arrow-head shows the chirality of charge propagation of that mode and $\nu = 0$ corresponds to the vacuum. For $\nu = 2/3$, we show the bare edge mode structure in (a) and the $1/3$ edge reconstruction (blue) [7] in (b).

modes have zero temperature, which is the contact temperature, and they are completely thermally isolated from the upstream modes. We assume that the particle-hole creation processes (which generate the noise) efficiently transfer heat energy among the modes at the noise spot to locally equilibrate those. This leads to a constant noise in the “No” thermal equilibration regime (Ref. 47 pointed out a length dependent noise based on a different limit).

IV. INSIGHT INTO THE RESULTS

Here, we qualitatively discuss a number of interesting features in the shot noise Fano factors, which we find by looking at the Table I and show their importance. In the following, we depict those sequentially pointing out the usefulness of each of those and relating one another:

1. F_1 vs. F_2 vs. F_c : The present article is based on the study of shot noise, therefore, immediate questions appear to a reader’s mind regarding the qualitative relations among the auto- and cross-correlation Fano factors and the sign of the cross-correlation.
 - (A) $F_1 = F_2$: Two auto-correlations are the same due to the current conservation.
 - (B) $F_c < 0$: A particle or hole can end up in either D_1 or D_2 , which keeps those drains to be anti-correlated, leading to a negative cross-correlation. Hence, the negative sign of F_c

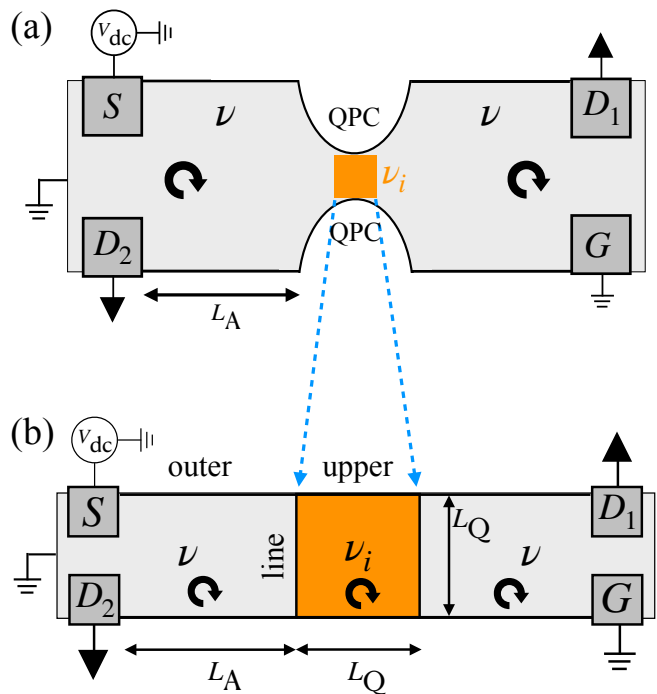


FIG. 2. An effective modeling of the QPC geometry (c.f. Fig. 1(a)) while we consider equilibration. We describe the chirality of charge propagation of each filling by the circular arrows. (a) We schematically show the QPC geometry, where ν and $\nu_i (< \nu)$ are the bulk and QPC filling factors respectively and L_A, L_Q are the geometric lengths with $L_Q \ll L_A$. (b) Effective model of the QPC geometry with edge equilibration for bulk filling ν and QPC filling ν_i . We show three distinct boundaries: the boundary of ν with vacuum as “outer”, the boundary of ν_i with vacuum as “upper”, and the boundary between ν and ν_i as “line”.

represents that the constituents of the noise reach different contacts.

- (C) $F_1 = F_2 \stackrel{?}{=} -F_c$: Having understood each of the auto- and cross-correlations individually, a natural question emerges as the inequalities among those. In addition, whether the nature of the bulk filling—being particle-like or hole-like—can play a role. Below we present a qualitative discussion.

We can write Eqs. (3) to (5) in a more simplified manner as $F_1 = F_2 = F_M + F_N + F_O + F_P$ and $F_c = -F_M - F_N + F'_O + F'_P$. If $\langle (\Delta I_S)^2 \rangle = \langle (\Delta I_G)^2 \rangle \approx 0$, then we have $F_O = F_P = F'_O = F'_P \approx 0$ leading to $F_1 = F_2 = -F_c$. This equality occurs for the $\nu =$ particle-like states as they contains co-propagating edges in the “outer” segments. Therefore, heat propagates only ballistically there which leads to the exponentially suppressed contributions from the O, P noise spots (Fig. 3(a)).

On the contrary, for the $\nu =$ hole-like states we have counter-propagating edge modes in

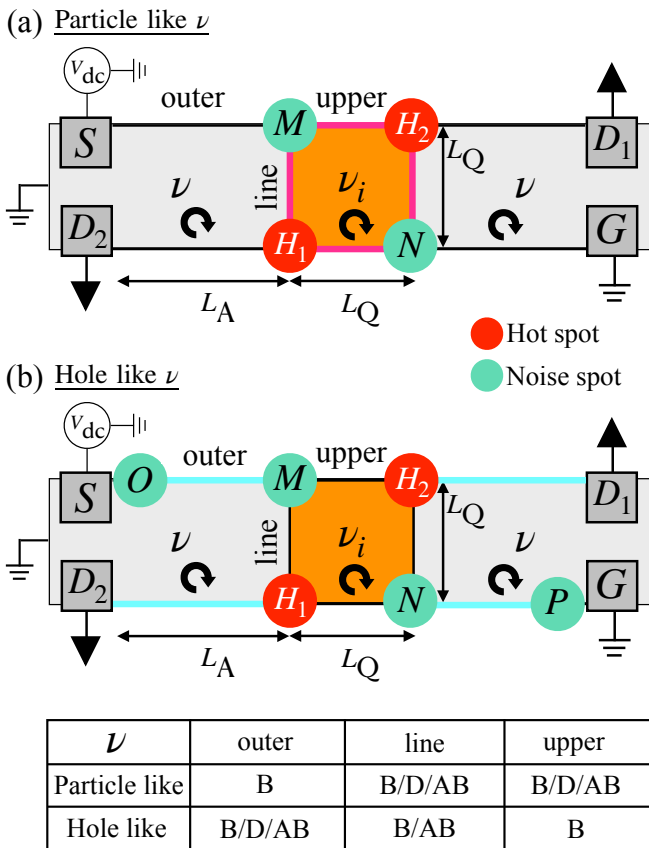


FIG. 3. We show the generation of hotspots (red circles) resulting in noise spots (green circles) while considering the equilibration for both the $\nu =$ particle-like and $\nu =$ hole-like filling fractions and the QPC has filling $\nu_i < \nu$. The chirality of charge propagation of each filling is depicted by the circular arrows. (a) We have ν as the particle-like filling fraction. The nature of heat transport is ballistic (“B”) in the “outer” segment and can be “B” or diffusive (“D”) or anti-ballistic (“AB”) in the “line” and “upper” segments. We have two hot spots as H_1, H_2 , which result in two noise spots as M, N . We note that the nature of heat transport in the “line” and “upper” segments (pink shaded lines) determine whether we have a constant noise or length-dependent noise. (b) We have ν as the hole-like filling fraction. The nature of heat transport can be “B” or “D” or “AB” in the “outer” segment, can be “B” or “AB” in the “line” segment, and is “B” in the “upper” segment. We have two hot spots as H_1, H_2 , which result in four noise spots as M, N, O, P . As there can be “D” or “AB” heat transport in the “outer” segment, hence we have additional noise spots O, P . We note that the nature of heat transport in the “outer” segment (cyan shaded lines) determine whether we have a constant noise or a length-dependent noise.

the “outer” segments. Therefore, heat can also propagate diffusively or antiballistically there which lead to constant contributions from the O, P noise spots as $\langle (\Delta I_S)^2 \rangle = \langle (\Delta I_G)^2 \rangle \neq 0$ (Fig. 3(b)). This leads to each of the F_O, F_P, F'_O, F'_P to be $\neq 0$ and hence

$F_1 = F_2 \neq -F_c$. Such inequalities are indeed found in recent experiments [48].

After learning the inequalities among the Fano factors, naturally we want to understand those in the quantitative level. While we give explicit numerical values in Table I for the Fano factors, however, one can qualitatively understand when the values of the Fano factors are close to zero or a constant or exhibit a length dependence. We discuss those in the following.

2. $F_1 = F_2 = -F_c \approx 0$:

If we have ballistic heat propagation along each of the “outer”, “line”, and “upper” segments, then heat can not reach efficiently from any hot spot to any noise spot. This leads to an exponentially suppressed contribution to the shot noise from each noise spot. Thereby, $F_M = F_N = F_O = F_P = F'_O = F'_P \approx 0$ leading to $F_1 = F_2 = -F_c \approx 0$.

3. $(F_1 = F_2, F_c) = \text{constant or } f(l_{\text{eq}}^{\text{th}}, L_Q, L_A)$:

If we have only ballistic or antiballistic heat transports along each of the segments of the QPC geometry, then heat can reach from any hot spot to any noise spot inefficiently or efficiently, respectively. Thereby, a zero or a constant contribution to the shot noise Fano factors can be attributed.

However, if the heat is transported diffusively through any segment then it reaches to the contacts very slowly along that segment. This gives rise to a length dependence in the temperatures of the hot spots. The length dependence has a functional form relating the geometric length of that segment and $l_{\text{eq}}^{\text{th}}$. The heat reaches from the hot spots to the noise spots and thus the noise spots also acquire that length scale dependence in their temperatures, which is manifested in the shot noises. From Table I we note that we have diffusive heat transports for $\{1, 1/3\}$ and $\{1, 2/3\}$ along “line” and “upper” segments respectively leading to a $\sqrt{l_{\text{eq}}^{\text{th}}/L_Q}$ dependence in the Fano factors. Similarly, for $\{2/3, 1/3\}$ and $\{2/3, [1/3]\}$ diffusive heat transports occur along the “outer” segment leading to a $\sqrt{L_A/l_{\text{eq}}^{\text{th}}}$ dependence in the Fano factors.

The final piece of our observations is to provide insights on how the bulk filling—being particle-like or hole-like— impacts different thermal equilibration regimes which in turn leaves its impression on the Fano factors. Below we show that interesting features arise and one can understand those in a qualitative level, keeping numerical values aside.

4. “No” = “Hybrid” \neq “Full” for $\nu =$ particle-like :

The difference between “No” and “Hybrid” thermal equilibration regimes is that all the edge

modes remain thermally unequilibrated in the former while they equilibrate in the latter only along the “outer” segment (c.f. Fig. 3(a)). Now, for the $\nu =$ particle-like states the heat transport along the “outer” segment is ballistic always since we have co-propagating modes. Hence, it does not matter if those modes in the “outer” segment thermally equilibrate or not, since they will not contribute to the shot noise leading to “No” = “Hybrid”. However, in the “Full” thermal equilibration regime the modes thermally equilibrate both along the “line” and “upper” segments (c.f. Fig. 3(a)) leading to “No” = “Hybrid” \neq “Full”.

5. “No” \neq “Hybrid” = “Full” for $\nu =$ hole-like :

A common fact between the “Hybrid” and “Full” thermal equilibration regimes is that the “outer” segment is thermally equilibrated for both and the heat transport along the “outer” segment is antiballistic (c.f. Fig. 3(b)). Therefore, no heat can reach to the drains from a hot spot. It does not matter if the “line” and “upper” segments (c.f. Fig. 3(b)) are thermally equilibrated (“Full”) or not (“Hybrid”), all the heat is transferred from a hot spot to the noise spots leading to “Hybrid” = “Full”. However, in the “No” thermal equilibration regime the modes are not thermally equilibrated along the “outer” segment. Hence the ballistic modes, connecting a hot spot to its nearest drain, leak some amount of heat to that drain leading to “No” \neq “Hybrid” = “Full”.

V. IMPORTANCE OF A “HYBRID” THERMAL EQUILIBRATION REGIME

The “Hybrid” thermal equilibration regime—defined by the separation of length scales $L_Q \ll l_{\text{eq}}^{\text{th}} \ll L_A$ —is a generic operating point of present-day QPC devices once we accept two robust experimental facts: (i) charge equilibrates much faster than heat ($I_{\text{eq}}^{\text{ch}} \ll I_{\text{eq}}^{\text{th}}$) and (ii) device arms are much longer than the QPC constriction ($L_Q \ll L_A$). In this window, charge is fully equilibrated everywhere, while heat equilibrates in the arms (“outer” segments) but not in the short region surrounding the QPC (“line”/“upper” segments). This spatially inhomogeneous equilibration is precisely what the “Hybrid” thermal equilibration regime encodes. It equips us with a controlled way to separate local QPC physics from long-arm heat transport, turning shot-noise at a conductance plateau into a nonlocal probe of edge hydrodynamics.

In particular, this raises a major concern in the experimental platform, asking the question of how deeply this regime affects the different measurement outcomes. We here provide a concrete answer and a principle that dictates that answer for the two different types of edges, namely particle-like edges and hole-like edges. In particle-like edges (co-propagating “outer” modes), “Hy-

brid” and “No” thermal equilibration give the same shot-noise outcomes, revealing that arm thermal equilibration is inert while QPC-region thermal equilibration matters. Conversely, in hole-like edges (counter-propagating “outer” modes), “Hybrid” and “Full” thermal equilibration coincide, exposing the arms as the relevant thermal bottleneck. Thus, the ‘Hybrid’ thermal equilibration regime sorts whether noise is controlled by the arms or by the QPC segment, which is also relevant for experiments involving QPC devices. Moreover, the “Hybrid” thermal equilibration regime asks future theory and experiment to treat thermal equilibration as segment-selective rather than uniform.

VI. COMPARISON WITH RECENT EXPERIMENTS

Our study assumes full charge equilibration in each segment of the QPC geometry, giving rise to well quantized QPC conductance plateaus. Such formation of QPC plateaus are robust and quite generally backed up by recent experiments [32, 34, 42, 49–53]. In this paper, we are only dealing with $\nu_i < \nu$ leading to a QPC plateau at ν_i/ν , however, cases with $\nu_i > \nu$ can also lead to a QPC plateau following charge equilibration as shown in Refs. 39 and 40. We stress that such mechanisms leading to quantized plateaus are not only tied with 2DEG systems [32, 34, 42, 49, 52] but also with recent studies in graphene systems [50, 51].

These plateaus are in general noisy, which is qualitatively consistent with Ref. 34. However, the auto-correlation Fano factors were found to be the same as the bulk filling in Ref. 34. In our study, for some cases, we have found the Fano factors are comparable but somewhat larger than in Ref. 34. For example, in the case $(\nu, \nu_i) = 3/5, 1/3$, we have $F_1 = F_2 \approx 0.53$ in “No” and “Hybrid” thermal equilibration regimes and in the case $(\nu, \nu_i) = 4/7, 1/3$, we have $F_1 = F_2 \approx 0.39$ in “No”, “Hybrid”, and “Full” thermal equilibration regimes (Table I). The measurement of cross-correlations can distinguish different thermal equilibration regimes, while the auto-correlations are same (Table I). We note a feature in our Table I for hole-like states and we point out that this is indeed consistent with recent experiments [48].

VII. SUMMARY AND FUTURE PROSPECTS

In this work, we have shown how the latest findings [35–38] of the inequality between charge and thermal equilibration lengths can affect the electrical shot noise. Our findings depict that distinct universal facets arise among the different thermal equilibration regimes for the edges of particle-like and hole-like fillings fractions. We have analyzed different Abelian quantum Hall states as the bulk filling (ν) and their known or possible QPC transmission plateaus (Table II). We have assumed full

charge equilibration throughout our analysis, which has licensed us in determining the transmission plateau for a given QPC filling ($\nu_i < \nu$). We have considered three different inequalities among the geometric lengths (L_A, L_Q) and the thermal equilibration lengths ($l_{\text{eq}}^{\text{th}}$). These three regimes of thermal equilibration have been denoted as “No” (both the arm and the edges around QPC are thermally unequilibrated), “Hybrid” (the arm is thermally equilibrated but not the edges around QPC), and “Full” (both the arm and the edges around QPC are thermally equilibrated). We have found for the particle-like states the thermal equilibration of the edges around the QPC affects the shot noise and for the hole-like states the thermal equilibration of the edges at the arms affects the shot noise (c.f. Table I and Fig. 3). We have found that the magnitude of the auto-correlation Fano factors is always larger than the cross-correlation Fano factor for the hole-like states, since the thermal transport contribution along the arm is either diffusive or antiballistic.

This work is a step in understanding how the shot noise is affected by different thermal equilibration regimes in a QPC geometry at a QPC transmission plateau. We note that the analyses are valid if we consider similar geometry made out of interfaces [18]. This work can be extended beyond the Abelian quantum Hall states to the non-Abelian fillings (e.g. $\nu = 12/5$ [54, 55]), where there are no extensive studies yet (recently $\nu = 5/2$ is considered [18]). In this work, we only focus on understanding the conventional QPC transmission plateau without the engineered interface modes. However, 2DEG interface QPC [56] is an intriguing direction that we hope to look into in the future. Another interesting direction will be the graphene quantum Hall effect. With the recent improvements and understandings, QPC and interfaces in graphene quantum Hall systems have become very relevant [57, 58]. We also note that in graphene how to construct a QPC is not unique, which makes the problem even richer. Interesting future directions may include other topological insulators (for example quantum spin Hall states) [11, 59, 60], quantum spin liquids [61–63], and more.

ACKNOWLEDGMENTS

We thank Moshe Goldstein and Yuval Gefen for many illuminating discussions. We thank Udit Khanna for useful discussions. S.M. was supported by the Weizmann Institute of Science, Israel Deans fellowship through Feinberg Graduate School and the senior postdoctoral fellowship, as well as the Raymond Beverly Sackler Center for Computational Molecular and Material Science at Tel Aviv University. A.D. was supported by DFG MI 658/10-2 and DFG RO 2247/11-1. A.D. also thanks the Israel Planning and budgeting committee (PBC) and the Weizmann Institute of Science, the Dean of Faculty fellowship, and the Koshland Foundation for financial support. A.D. thanks IISER Tirupati start up grant for support.

Appendix A: Derivations of $\delta^2 I_1, \delta^2 I_2, \delta^2 I_c$

We follow Refs. 18, 20, 39, and 40 and re-derive the expressions of $\delta^2 I_1, \delta^2 I_2, \delta^2 I_c$ explaining each term in full details which will help to follow our entire calculations in the main manuscript. We assume that the geometric lengths are larger than the charge equilibration length leading to $(L_A, L_Q) \gg l_{\text{eq}}^{\text{ch}}$.

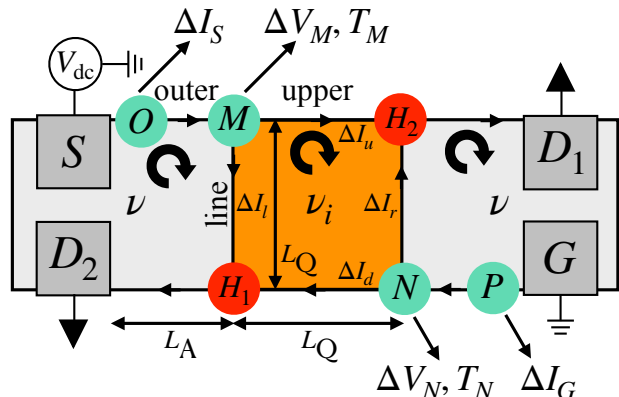


FIG. 4. A Hall bar device with bulk filling ν and QPC filling $\nu_i (< \nu)$ with a source S (biased by a dc voltage V_{dc}), a ground contact G , and two drains, D_1 and D_2 . The geometric lengths are L_A, L_Q . We denote the segment between the vacuum and ν as “outer”, between the vacuum and ν_i as “upper”, and between ν and ν_i as “line”. The arrow shows the fully equilibrated charge propagation along each segment while the circular arrow depicts the chirality of each filling. Hot spots H_1, H_2 (red circles) are created due to the voltage drops which are responsible for the creation of noise spots M, N, O, P (green circles) [20].

We write the following equations for the current fluctuations as

$$\begin{aligned} \Delta I_1 &= \Delta I_u + \Delta I_r, \\ \Delta I_2 &= \Delta I_d + \Delta I_l, \\ \Delta I_S &= \Delta I_u + \Delta I_l, \\ \Delta I_G &= \Delta I_d + \Delta I_r, \end{aligned} \quad (\text{A1})$$

and

$$\begin{aligned} \Delta I_l &= (\nu - \nu_i) \frac{e^2}{h} \Delta V_M + \Delta I_l^{\text{th}}, \\ \Delta I_u &= \nu_i \frac{e^2}{h} \Delta V_M + \Delta I_u^{\text{th}}, \\ \Delta I_r &= (\nu - \nu_i) \frac{e^2}{h} \Delta V_N + \Delta I_r^{\text{th}}, \\ \Delta I_d &= \nu_i \frac{e^2}{h} \Delta V_N + \Delta I_d^{\text{th}}. \end{aligned} \quad (\text{A2})$$

Hence, we find

$$\begin{aligned}\Delta I_1 &= \nu_i \frac{e^2}{h} \Delta V_M + \Delta I_u^{\text{th}} + (\nu - \nu_i) \frac{e^2}{h} \Delta V_N + \Delta I_r^{\text{th}} \\ &= \frac{\nu_i}{\nu} \Delta I_S + \frac{(\nu - \nu_i)}{\nu} \Delta I_G \\ &\quad + \frac{(\nu - \nu_i)}{\nu} (\Delta I_u^{\text{th}} - \Delta I_d^{\text{th}}) + \frac{\nu_i}{\nu} (\Delta I_r^{\text{th}} - \Delta I_l^{\text{th}})\end{aligned}\quad (\text{A3})$$

and

$$\begin{aligned}\Delta I_2 &= \frac{\nu_i}{\nu} \Delta I_G + \frac{(\nu - \nu_i)}{\nu} \Delta I_S \\ &\quad + \frac{(\nu - \nu_i)}{\nu} (\Delta I_d^{\text{th}} - \Delta I_u^{\text{th}}) + \frac{\nu_i}{\nu} (\Delta I_l^{\text{th}} - \Delta I_r^{\text{th}}).\end{aligned}\quad (\text{A4})$$

We use the local Johnson-Nyquist relations for thermal noise as

$$\begin{aligned}\langle (\Delta I_l^{\text{th}})^2 \rangle &= \frac{2e^2}{h} (\nu - \nu_i) k_B T_M, \\ \langle (\Delta I_u^{\text{th}})^2 \rangle &= \frac{2e^2}{h} \nu_i k_B T_M, \\ \langle (\Delta I_r^{\text{th}})^2 \rangle &= \frac{2e^2}{h} (\nu - \nu_i) k_B T_N, \\ \langle (\Delta I_d^{\text{th}})^2 \rangle &= \frac{2e^2}{h} \nu_i k_B T_N, \\ \langle (\Delta I_i^{\text{th}} \Delta I_j^{\text{th}}) \rangle &= 0, \text{ for } i \neq j \text{ and } i, j \in \{l, u, r, d\},\end{aligned}\quad (\text{A5})$$

and find the correlations to be

$$\begin{aligned}\delta^2 I_1 &= 2 \left(\frac{e^2}{h} \right) \frac{\nu_i}{\nu} (\nu - \nu_i) k_B (T_M + T_N) \\ &\quad + \frac{1}{\nu^2} \left[\nu_i^2 \langle (\Delta I_S)^2 \rangle + (\nu - \nu_i)^2 \langle (\Delta I_G)^2 \rangle \right],\end{aligned}\quad (\text{A6})$$

$$\begin{aligned}\delta^2 I_2 &= 2 \left(\frac{e^2}{h} \right) \frac{\nu_i}{\nu} (\nu - \nu_i) k_B (T_M + T_N) \\ &\quad + \frac{1}{\nu^2} \left[\nu_i^2 \langle (\Delta I_G)^2 \rangle + (\nu - \nu_i)^2 \langle (\Delta I_S)^2 \rangle \right],\end{aligned}\quad (\text{A7})$$

and

$$\begin{aligned}\delta^2 I_c &= -2 \left(\frac{e^2}{h} \right) \frac{\nu_i}{\nu} (\nu - \nu_i) k_B (T_M + T_N) \\ &\quad + \frac{\nu_i (\nu - \nu_i)}{\nu^2} \left[\langle (\Delta I_G)^2 \rangle + \langle (\Delta I_S)^2 \rangle \right],\end{aligned}\quad (\text{A8})$$

where T_M, T_N are, respectively, the temperatures at the noise spots M and N . The computation of T_M, T_N requires the nature of heat transport along each segment of the device. Below we consider a particular case to show how T_M, T_N are calculated by solving self-consistent equilibration equations and considering energy conservation at each edge mode junction [18, 20].

Appendix B: Computation of T_M, T_N

We show the detailed calculation of T_M, T_N when charge and heat are fully equilibrated in each segment of the device (leading to $(L_A, L_Q) \gg l_{\text{eq}}^{\text{ch}}$ and $(L_A, L_Q) \gg l_{\text{eq}}^{\text{th}}$) and the heat transport is ballistic in “outer”, antiballistic in “line”, and ballistic in “upper” segments (Fig. 5). Other cases can be derived in a similar manner.

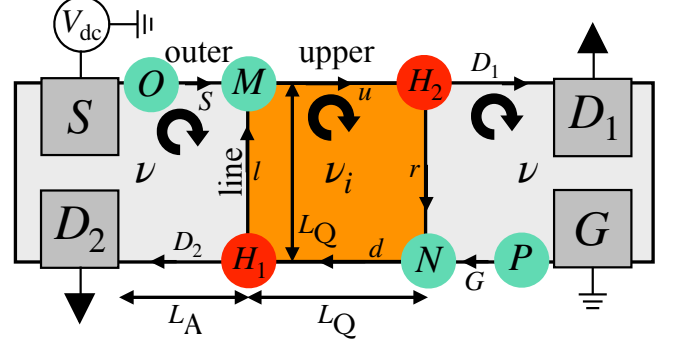


FIG. 5. We assume charge to be fully equilibrated leading to ballistic transport, moving “downstream” along each segment of the device. Each circular arrow shows the chirality of charge propagation of the respective filling ($\nu > \nu_i$). The direction opposite to charge flow (“upstream”) is taken as antiballistic. Heat is also fully equilibrated and we show here the case when the heat transport is ballistic in “outer”, antiballistic in “line”, and ballistic in “upper” segments, as shown by the arrows. Voltage drops occur at the hot spots H_1, H_2 (red circles), giving rise to the noise spots M, N, O, P (green circles) [20].

We calculate T_M, T_N assuming zero temperature in the contacts/leads. We write the energy conservation equations at H_1, N, H_2, M as [20]

$$\begin{aligned}J_{D_2} + J_l &= P_{H_1} + J_d, \\ J_G + J_r &= J_d, \\ J_{D_1} + J_r &= P_{H_2} + J_u, \\ J_S + J_l &= J_u,\end{aligned}\quad (\text{B1})$$

where we have J_i as the heat current along $i \in \{S, G, D_1, D_2, u, r, d, l\}$ th segment, and P_{H_1}, P_{H_2} as, respectively, the powers dissipated in the hot spots H_1, H_2 .

We write the following expressions as

$$\begin{aligned}J_S &= 0, \quad J_u = \frac{\kappa}{2} T_M^2 (\delta c)_u, \quad J_{D_1} = \frac{\kappa}{2} T_{H_2}^2 (\delta c)_1, \\ J_G &= 0, \quad J_d = \frac{\kappa}{2} T_N^2 (\delta c)_d, \quad J_{D_2} = \frac{\kappa}{2} T_{H_1}^2 (\delta c)_2, \\ J_l &= \frac{\kappa}{2} T_{H_1}^2 (\delta c)_l, \quad J_r = \frac{\kappa}{2} T_{H_2}^2 (\delta c)_r,\end{aligned}\quad (\text{B2})$$

where $\kappa = \frac{\pi^2 k_B^2}{3h}$. Here, $T_M, T_N, T_{H_1}, T_{H_2}$ are the temperatures at M, N, H_1, H_2 respectively. P_{H_1}, P_{H_2} are the powers dissipated due to the Joule heating corresponding to the associated voltage drop at H_1, H_2 , respectively. We derive its explicit expression later and find

$P_{H_1} = P_{H_2}$. We have $(\delta c)_i = |(c_{\text{down}} - c_{\text{up}})_i|$ as the modulus of difference between the central charges of downstream and upstream modes in the i th segment. We write

$$\begin{aligned} \frac{\kappa}{2} T_{H_1}^2 (\delta c)_2 + \frac{\kappa}{2} T_{H_1}^2 (\delta c)_l &= P_{H_1} + \frac{\kappa}{2} T_N^2 (\delta c)_d, \\ 0 + \frac{\kappa}{2} T_{H_2}^2 (\delta c)_r &= \frac{\kappa}{2} T_N^2 (\delta c)_d, \\ \frac{\kappa}{2} T_{H_2}^2 (\delta c)_1 + \frac{\kappa}{2} T_{H_2}^2 (\delta c)_r &= P_{H_2} + \frac{\kappa}{2} T_M^2 (\delta c)_u, \\ 0 + \frac{\kappa}{2} T_{H_1}^2 (\delta c)_l &= \frac{\kappa}{2} T_M^2 (\delta c)_u, \end{aligned} \quad (\text{B3})$$

and therefore,

$$\begin{aligned} \frac{[(\delta c)_1 + (\delta c)_r]}{(\delta c)_r} (\delta c)_d \frac{\kappa}{2} T_N^2 &= P_{H_2} + \frac{\kappa}{2} (\delta c)_u T_M^2, \\ \frac{[(\delta c)_2 + (\delta c)_l]}{(\delta c)_l} (\delta c)_u \frac{\kappa}{2} T_M^2 &= P_{H_1} + \frac{\kappa}{2} (\delta c)_d T_N^2. \end{aligned} \quad (\text{B4})$$

This leads to

$$\begin{aligned} \frac{\kappa}{2} (\delta c)_u T_M^2 \left[1 + \frac{(\delta c)_2 + (\delta c)_l}{(\delta c)_l} \right] \\ = \frac{\kappa}{2} (\delta c)_d T_N^2 \left[1 + \frac{(\delta c)_1 + (\delta c)_r}{(\delta c)_r} \right]. \end{aligned} \quad (\text{B5})$$

We have $(\delta c)_u = (\delta c)_d$, $(\delta c)_2 = (\delta c)_1$, $(\delta c)_l = (\delta c)_r$, and hence $T_M = T_N$. Thereby,

$$\frac{\kappa T_M^2}{2} \frac{(\delta c)_1}{(\delta c)_r} (\delta c)_d = P_{H_2}, \quad (\text{B6})$$

leading to

$$T_M = T_N = \sqrt{\frac{2P_{H_2}}{\kappa} \frac{(\delta c)_r}{(\delta c)_1 (\delta c)_d}}. \quad (\text{B7})$$

Appendix C: Computation of $P_{H_1} = P_{H_2}$

We refer to Fig. 4 (assuming that the geometric lengths are larger than the charge equilibration length leading to $(L_A, L_Q) \gg l_{\text{eq}}^{\text{ch}}$) and write the electrical current conservation equations at M, N, H_1, H_2 respectively as

$$\begin{aligned} V_{\text{dc}} &= V_M, \\ V_N &= 0, \\ (\nu - \nu_i) V_M &= \nu V_{H_1}, \\ \nu_i V_M &= \nu V_{H_2}. \end{aligned} \quad (\text{C1})$$

We find

$$V_{H_1} = \frac{(\nu - \nu_i)}{\nu} V_{\text{dc}}, V_{H_2} = \frac{\nu_i}{\nu} V_{\text{dc}}. \quad (\text{C2})$$

The dissipated power at H_1 is

$$\begin{aligned} P_{H_1} &= \frac{e^2}{2h} \left[(\nu - \nu_i) V_M^2 + \nu_i^2 V_N^2 - \nu V_{H_1}^2 \right] \\ &= \frac{e^2 V_{\text{dc}}^2}{h} \frac{\nu_i (\nu - \nu_i)}{2\nu}. \end{aligned} \quad (\text{C3})$$

Similar calculations show $P_{H_1} = P_{H_2}$.

Appendix D: Calculation of $\langle (\Delta I_S)^2 \rangle = \langle (\Delta I_G)^2 \rangle$

We consider two counter-propagating modes in a quantum Hall edge, where inter-mode charge tunneling happens. Shot noise occurs while electric current is partitioned. The fluctuation of local tunneling current has two parts as

$$\Delta I_j^\tau = \Delta I_j^{\tau, \text{th}} + \Delta I_j^{\tau, \text{v}}. \quad (\text{D1})$$

Here, $\Delta I_j^{\tau, \text{th}}$ is the fluctuation for the local Johnson-Nyquist noise with

$$\langle \Delta I_j^{\tau, \text{th}} \Delta I_j^{\tau, \text{th}} \rangle = \frac{2e^2}{h} g k_B (T_{+,j} + T_{-,j}), \quad (\text{D2})$$

where g is the tunneling coupling between the two modes having local temperatures $T_{+,j}$ and $T_{-,j}$ at j th location.

We have

$$\Delta I_j^{\tau, \text{v}} = g \frac{e^2}{h} (\Delta V_{+,j} - \Delta V_{-,j}), \quad (\text{D3})$$

where the two modes having local voltages $V_{+,j}$ and $V_{-,j}$ at j th location.

We take the continuum limit and find the expression for the noise profile [16, 20] as written in Eq. (7) of the main text.

Appendix E: Temperature profiles $T_+(x), T_-(x)$

The local temperature profiles of the modes are computed by solving the following differential equation [20].

$$\partial_x \begin{pmatrix} T_+^2(x) \\ T_-^2(x) \end{pmatrix} \sim \frac{1}{l} \begin{pmatrix} -n_u & n_u \\ -n_d & n_d \end{pmatrix} \begin{pmatrix} T_+^2(x) \\ T_-^2(x) \end{pmatrix} + P_J, \quad (\text{E1})$$

where P_J is the power dissipation due to Joule heating and n_u, n_d are respectively the total number of upstream and downstream modes and $l \propto l_{\text{eq}}^{\text{th}}$. We have distinct solutions of this equation for different heat transport—ballistic, antiballistic, diffusive. These distinct solutions, while inserted in Fig. 5, lead to different noise profiles.

- [1] D. C. Tsui, H. L. Stormer, and A. C. Gossard, Two-dimensional magnetotransport in the extreme quantum limit, *Phys. Rev. Lett.* **48**, 1559 (1982).
- [2] R. B. Laughlin, Anomalous quantum hall effect: An incompressible quantum fluid with fractionally charged excitations, *Phys. Rev. Lett.* **50**, 1395 (1983).
- [3] M. Z. Hasan and C. L. Kane, Colloquium: Topological insulators, *Rev. Mod. Phys.* **82**, 3045 (2010).
- [4] T. H. Hansson, M. Hermanns, S. H. Simon, and S. F. Viefers, Quantum hall physics: Hierarchies and conformal field theory techniques, *Rev. Mod. Phys.* **89**, 025005 (2017).
- [5] C.-Z. Chang, C.-X. Liu, and A. H. MacDonald, Colloquium: Quantum anomalous hall effect, *Rev. Mod. Phys.* **95**, 011002 (2023).
- [6] X. G. Wen, Gapless boundary excitations in the quantum hall states and in the chiral spin states, *Phys. Rev. B* **43**, 11025 (1991).
- [7] J. Wang, Y. Meir, and Y. Gefen, Edge reconstruction in the $\nu=2/3$ fractional quantum hall state, *Phys. Rev. Lett.* **111**, 246803 (2013).
- [8] U. Khanna, M. Goldstein, and Y. Gefen, Fractional edge reconstruction in integer quantum hall phases, *Phys. Rev. B* **103**, L121302 (2021).
- [9] U. Khanna, M. Goldstein, and Y. Gefen, Emergence of neutral modes in Laughlin-like fractional quantum hall phases, *Phys. Rev. Lett.* **129**, 146801 (2022).
- [10] U. Khanna, G. Murthy, S. Rao, and Y. Gefen, Spin mode switching at the edge of a quantum hall system, *Phys. Rev. Lett.* **119**, 186804 (2017).
- [11] U. Khanna, Y. Gefen, O. Entin-Wohlman, and A. Aharony, Edge reconstruction of a time-reversal invariant insulator: Compressible-incompressible stripes, *Phys. Rev. Lett.* **128**, 186801 (2022).
- [12] C. d. C. Chamon and X. G. Wen, Sharp and smooth boundaries of quantum hall liquids, *Phys. Rev. B* **49**, 8227 (1994).
- [13] U. Khanna, M. Goldstein, and Y. Gefen, Edge reconstruction and emergent neutral modes in integer and fractional quantum hall phases, *Low Temperature Physics* **48**, 420 (2022).
- [14] I. Protopopov, Y. Gefen, and A. Mirlin, Transport in a disordered $\nu = 2/3$ fractional quantum hall junction, *Annals of Physics* **385**, 287 (2017).
- [15] C. Spånslätt, J. Park, Y. Gefen, and A. D. Mirlin, Topological classification of shot noise on fractional quantum hall edges, *Phys. Rev. Lett.* **123**, 137701 (2019).
- [16] J. Park, A. D. Mirlin, B. Rosenow, and Y. Gefen, Noise on complex quantum hall edges: Chiral anomaly and heat diffusion, *Phys. Rev. B* **99**, 161302 (2019).
- [17] J. Park, C. Spånslätt, Y. Gefen, and A. D. Mirlin, Noise on the non-abelian $\nu = 5/2$ fractional quantum hall edge, *Phys. Rev. Lett.* **125**, 157702 (2020).
- [18] S. Manna, A. Das, M. Goldstein, and Y. Gefen, Full classification of transport on an equilibrated $5/2$ edge via shot noise, *Phys. Rev. Lett.* **132**, 136502 (2024).
- [19] C. Nosiiglia, J. Park, B. Rosenow, and Y. Gefen, Incoherent transport on the $\nu = 2/3$ quantum hall edge, *Phys. Rev. B* **98**, 115408 (2018).
- [20] C. Spånslätt, J. Park, Y. Gefen, and A. D. Mirlin, Conductance plateaus and shot noise in fractional quantum hall point contacts, *Phys. Rev. B* **101**, 075308 (2020).
- [21] C. Spånslätt, Y. Gefen, I. V. Gornyi, and D. G. Polyakov, Contacts, equilibration, and interactions in fractional quantum hall edge transport, *Phys. Rev. B* **104**, 115416 (2021).
- [22] T. Martin and R. Landauer, Wave-packet approach to noise in multichannel mesoscopic systems, *Phys. Rev. B* **45**, 1742 (1992).
- [23] T. Martin, Noise in mesoscopic physics, *arXiv:cond-mat/0501208* (2005).
- [24] R. de Picciotto, M. Reznikov, M. Heiblum, V. Umansky, G. Bunin, and D. Mahalu, Direct observation of a fractional charge, *Nature* **389**, 162 (1997).
- [25] L. Saminadayar, D. C. Glattli, Y. Jin, and B. Etienne, Observation of the $e/3$ fractionally charged Laughlin quasiparticle, *Phys. Rev. Lett.* **79**, 2526 (1997).
- [26] R. de Picciotto, M. Reznikov, M. Heiblum, V. Umansky, G. Bunin, and D. Mahalu, Direct observation of a fractional charge, *Physica B: Condensed Matter* **249-251**, 395 (1998).
- [27] M. Reznikov, R. de Picciotto, M. Heiblum, D. C. Glattli, A. Kumar, and L. Saminadayar, Quantum shot noise, *Superlattices and Microstructures* **23**, 901 (1998).
- [28] N. Batra and D. E. Feldman, Different fractional charges from auto- and cross-correlation noise in quantum hall states without upstream modes, *Phys. Rev. Lett.* **132**, 226601 (2024).
- [29] E. Grosfeld and S. Das, Probing the neutral edge modes in transport across a point contact via thermal effects in the read-rezayi non-abelian quantum hall states, *Phys. Rev. Lett.* **102**, 106403 (2009).
- [30] J. Park, B. Rosenow, and Y. Gefen, Symmetry-related transport on a fractional quantum hall edge, *Phys. Rev. Res.* **3**, 023083 (2021).
- [31] S. Biswas, R. Bhattacharyya, H. K. Kundu, A. Das, M. Heiblum, V. Umansky, M. Goldstein, and Y. Gefen, Shot noise does not always provide the quasiparticle charge, *Nature Physics* **18**, 1476 (2022).
- [32] R. Sabo, I. Gurman, A. Rosenblatt, F. Lafont, D. Banitt, J. Park, M. Heiblum, Y. Gefen, V. Umansky, and D. Mahalu, Edge reconstruction in fractional quantum hall states, *Nature Physics* **13**, 491 (2017).
- [33] A. Bid, N. Ofek, H. Inoue, M. Heiblum, C. L. Kane, V. Umansky, and D. Mahalu, Observation of neutral modes in the fractional quantum hall regime, *Nature* **466**, 585 (2010).
- [34] R. Bhattacharyya, M. Banerjee, M. Heiblum, D. Mahalu, and V. Umansky, Melting of interference in the fractional quantum hall effect: Appearance of neutral modes, *Phys. Rev. Lett.* **122**, 246801 (2019).
- [35] S. K. Srivastav, R. Kumar, C. Spånslätt, K. Watanabe, T. Taniguchi, A. D. Mirlin, Y. Gefen, and A. Das, Vanishing thermal equilibration for hole-conjugate fractional quantum hall states in graphene, *Phys. Rev. Lett.* **126**, 216803 (2021).
- [36] R. A. Melcer, B. Dutta, C. Spånslätt, J. Park, A. D. Mirlin, and V. Umansky, Absent thermal equilibration on fractional quantum hall edges over macroscopic scale, *Nature Communications* **13**, 376 (2022).
- [37] R. Kumar, S. K. Srivastav, C. Spånslätt, K. Watanabe, T. Taniguchi, Y. Gefen, A. D. Mirlin, and A. Das, Obser-

- vation of ballistic upstream modes at fractional quantum hall edges of graphene, *Nature Communications* **13**, 213 (2022).
- [38] S. K. Srivastav, R. Kumar, C. Spånslätt, K. Watanabe, T. Taniguchi, A. D. Mirlin, Y. Gefen, and A. Das, Determination of topological edge quantum numbers of fractional quantum hall phases by thermal conductance measurements, *Nature Communications* **13**, 5185 (2022).
- [39] S. Manna, A. Das, Y. Gefen, and M. Goldstein, Shot noise as a diagnostic in the $\nu = 2/3$ fractional quantum Hall edge zoo, *Low Temperature Physics* **50**, 1113 (2024).
- [40] S. Manna, A. Das, Y. Gefen, and M. Goldstein, Multiple mechanisms for emerging conductance plateaus in fractional quantum Hall states, *Phys. Rev. Lett.* **134**, 256503 (2025).
- [41] We define the time average of an operator x as $\langle x \rangle = \lim_{\tau \rightarrow \infty} \frac{1}{\tau} \int_{-\tau}^{\tau} x(t) dt$.
- [42] J. Nakamura, S. Liang, G. C. Gardner, and M. J. Manfra, Half-integer conductance plateau at the $\nu = 2/3$ fractional quantum hall state in a quantum point contact, *Phys. Rev. Lett.* **130**, 076205 (2023).
- [43] H. Bartolomei, M. Kumar, R. Bisognin, A. Marguerite, J.-M. Berroir, E. Bocquillon, B. Plaças, A. Cavanna, Q. Dong, U. Gennser, Y. Jin, and G. Fève, Fractional statistics in anyon collisions, *Science* **368**, 173 (2020).
- [44] J.-Y. M. Lee, C. Hong, T. Alkalay, N. Schiller, V. Umansky, M. Heiblum, Y. Oreg, and H.-S. Sim, Partitioning of diluted anyons reveals their braiding statistics, *Nature* **617**, 277 (2023).
- [45] M. Banerjee, M. Heiblum, V. Umansky, D. E. Feldman, Y. Oreg, and A. Stern, Observation of half-integer thermal hall conductance, *Nature* **559**, 205 (2018).
- [46] A. Aharon-Steinberg, Y. Oreg, and A. Stern, Phenomenological theory of heat transport in the fractional quantum hall effect, *Phys. Rev. B* **99**, 041302 (2019).
- [47] J. Park, C. Spånslätt, and A. D. Mirlin, Fingerprints of anti-pfaffian topological order in quantum point contact transport, *Phys. Rev. Lett.* **132**, 256601 (2024).
- [48] C. Glattli, (private communication showing their unpublished auto- and cross-correlation data are indeed unequal).
- [49] A. Bid, N. Ofek, M. Heiblum, V. Umansky, and D. Mahalu, Shot noise and charge at the $2/3$ composite fractional quantum hall state, *Phys. Rev. Lett.* **103**, 236802 (2009).
- [50] K. Zimmermann, A. Jordan, F. Gay, K. Watanabe, T. Taniguchi, Z. Han, V. Bouchiat, H. Sellier, and B. Sacépé, Tunable transmission of quantum hall edge channels with full degeneracy lifting in split-gated graphene devices, *Nature Communications* **8**, 14983 (2017).
- [51] P. Pandey, S. Manna, K. N. Frei, J. Saji, A. Denis, A. Savin, K. Watanabe, T. Taniguchi, P. J. Hakonen, A. Das, and M. Kumar, Half-quantized hall plateaus in the confined geometry of graphene, [arXiv:2410.03896](https://arxiv.org/abs/2410.03896) (2024).
- [52] M. H. Fauzi, K. Nakagawara, K. Hashimoto, N. Shibata, and Y. Hirayama, Synthesizing $2h/e^2$ resistance plateau at the first landau level confined in a quantum point contact, [arXiv:2301.07488](https://arxiv.org/abs/2301.07488) (2023).
- [53] U. Roy, S. Manna, S. Chakraborty, K. Watanabe, T. Taniguchi, A. Das, M. Goldstein, Y. Gefen, and A. Das, Half-integer thermal conductance in the absence of Majorana mode, [arXiv:2506.12526](https://arxiv.org/abs/2506.12526) (2025).
- [54] N. Read and E. Rezayi, Beyond paired quantum hall states: Parafermions and incompressible states in the first excited landau level, *Phys. Rev. B* **59**, 8084 (1999).
- [55] M. Yutushui and D. F. Mross, Identifying non-abelian anyons with upstream noise, *Phys. Rev. B* **108**, L241102 (2023).
- [56] S. Biswas, H. K. Kundu, V. Umansky, and M. Heiblum, Electron pairing of interfering interface-based edge modes, *Phys. Rev. Lett.* **131**, 096302 (2023).
- [57] Y. Ronen, T. Werkmeister, D. H. Najafabadi, A. T. Pierce, L. E. Anderson, Y. J. Shin, S. Y. Lee, Y. H. Lee, B. Johnson, K. Watanabe, T. Taniguchi, A. Yacoby, and P. Kim, Aharonov–bohm effect in graphene-based fabry–pérot quantum hall interferometers, *Nature Nanotechnology* **16**, 563 (2021).
- [58] A. K. Paul, M. R. Sahu, K. Watanabe, T. Taniguchi, J. K. Jain, G. Murthy, and A. Das, Electrically switchable tunneling across a graphene pn junction: evidence for canted antiferromagnetic phase in $\nu = 0$ state, [arXiv:2205.00710](https://arxiv.org/abs/2205.00710) (2022).
- [59] J. Wang, Y. Meir, and Y. Gefen, Spontaneous breakdown of topological protection in two dimensions, *Phys. Rev. Lett.* **118**, 046801 (2017).
- [60] N. John, A. D. Maestro, and B. Rosenow, Robustness of helical edge states under edge reconstruction, *Europhysics Letters* **140**, 26002 (2022).
- [61] A. Kitaev, Anyons in an exactly solved model and beyond, *Annals of Physics* **321**, 2 (2006).
- [62] A. Banerjee, C. A. Bridges, J. Q. Yan, A. A. Aczel, L. Li, M. B. Stone, G. E. Granroth, M. D. Lumsden, Y. Yiu, J. Knolle, S. Bhattacharjee, D. L. Kovrizhin, R. Moessner, D. A. Tennant, D. G. Mandrus, and S. E. Nagler, Proximate kitaev quantum spin liquid behaviour in a honeycomb magnet, *Nature Materials* **15**, 733 (2016).
- [63] Y. Kasahara, T. Ohnishi, Y. Mizukami, O. Tanaka, S. Ma, K. Sugii, N. Kurita, H. Tanaka, J. Nasu, Y. Motome, T. Shibauchi, and Y. Matsuda, Majorana quantization and half-integer thermal quantum hall effect in a kitaev spin liquid, *Nature* **559**, 227 (2018).